Application Note

Microbiology

Agilent

Trusted Answers

Efficacy of a Novel Confocal Imaging Reader for Evaluating Bacterial Biofilms

Author

Wendy Goodrich,
Agilent Technologies, Inc.

Abstract

Bacterial biofilms are complex communities of microorganisms organized within a self- or host-propagating extracellular substrate and can present with beneficial and/or detrimental results in natural environments and on many critical abiotic surfaces. Understanding the formation, development, components, and mechanisms of this bacterial way of life continues to be important to numerous fields of study and often requires a multidisciplinary approach that relies on several dedicated instruments to acquire data for analysis. This, in addition to their three-dimensional (3D) architecture, makes biofilms a particularly suitable model for evaluating the utility of a novel confocal imaging reader for analyzing them. The Agilent BioTek Cytation C10 confocal imaging reader is specifically built to integrate the functionality of up to five different instruments in one device, including both widefield and confocal imaging capabilities. This permits a broad choice of assays during experimental design while simultaneously supporting an orthogonal method. A variety of detection, imaging, and analysis methods enabled by the Cytation C10 are demonstrated in this application note using multiple bacterial strains and common biofilm assays.

Introduction

It is generally understood that bacteria prefer to live a communal lifestyle encased in a 3D extracellular matrix composed of a mix of extracellular polymeric substances (EPS). This architecture has been shown to consist of several microenvironments and is adaptable depending on conditions found in the surrounding host.[31] Bacteria undergo distinct phenotypic changes that make them highly proficient and opportunistic at building and maintaining these biofilm communities in diverse, and even extreme, habitats.[1, 7, 25] In addition to their ubiquitous presence in the natural world, human-built environments provide vast niches for bacteria to establish biofilms, and they are researched over many scientific disciplines due to the diverse roles biofilms play. Such roles include pathogenic, protective, or therapeutic actors in human and environmental health and disease, causative and preventative spoilage mechanisms in the cultivation and production of food products, toxic soil and marine remediation agents, or as vehicles in biofouling and corrosion in water- and fuel-processing infrastructures that support our daily needs.

Over the past four to five decades, the field of biofilm science has grown to include numerous different species and experimental conditions. This has resulted in paradigm shifts of understanding, notably in describing biofilm structure and function as well as the biofilm life cycle itself.[11, 17] Parallel to this, many novel biomaterials and technologies have been, or are being, developed or employed to gain insight into unanswered questions or solve urgent problems related to biofilms. However, in vitro methods using indirect and/or direct biochemical and imaging assays that rely on absorbance, fluorescence, luminescence detection, and/or widefield and confocal microscopy, continue to be fundamental in experimental design of biofilm systems, and are widely cited in biofilm literature.[1, 4, 5, 6] These tools are particularly useful during biofilm model development—a process that depends on the testing and optimization of numerous and diverse variables and outcomes, starting with the fundamental choice of bacterial species, whether it forms a biofilm, and the conditions under which this occurs. Additional experimental parameters may include:

- Investigating the effects of different growth nutrients and substrates on biofilm development;
- Determining optimal concentrations of stains, dyes, and other reagents or compounds;
- Selecting effective methods to measure response to genetic manipulations or other exposures such as to surfactants, pharmaceutical compounds, or toxins;
- Determining changes in phenotype between planktonic cells and mono and polymicrobial community life;
- Determining the results of applied external pressures like fluctuations in shear stress, temperature, pH, oxygen, or ionic charge at any or all points along a biofilm lifecycle.

These stages of model development exist regardless of research novelty, and can result in protocols for defining reproducible ground truths that are important when translating common models to pioneering ones. They are also important when generating foundational data that can inform on downstream experimental direction.

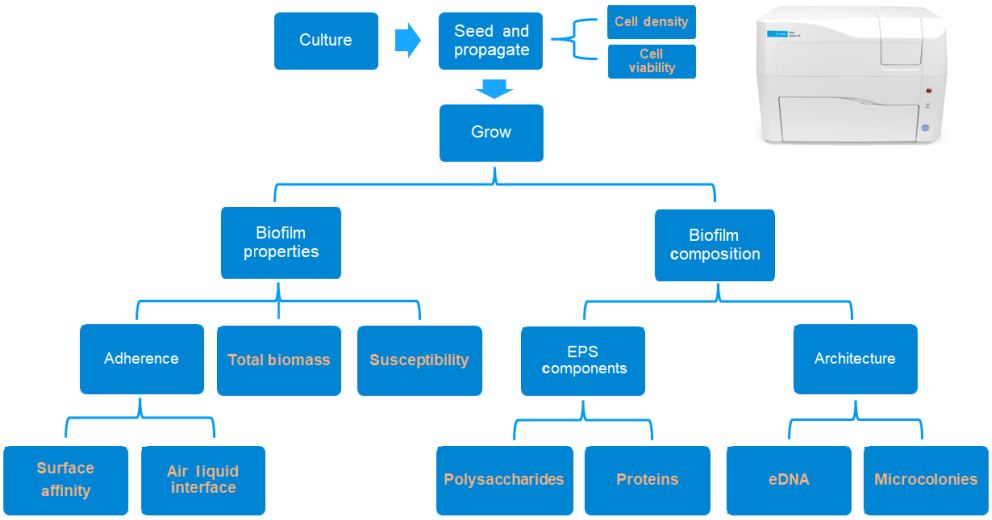

Figure 1. Overview of the biofilm evaluation workflow using the Agilent BioTek Cytation C10 confocal imaging reader (upper right). Descriptive text is in white, and the described experimental assays and/or end points are in orange.

This application note presents representative results from a collection of biofilm case studies, performed to evaluate the potential of the novel Cytation C10 confocal imaging reader as a tool for biofilm characterization. An overview of the evaluation workflow is shown in Figure 1.

Biofilms were assessed for properties such as surface affinity and growth characteristics, in addition to compositional features, including components and architecture of the EPS. The Cytation C10 proved to have multiple features conducive to biofilm analysis, as realized by the capability of the instrument to perform the detection and imaging techniques required by the various in vitro biofilm assays described herein. Having this functionality available in one device centralized both protocol definition and data management via a single user interface while allowing the choice of a wide range of detection and staining reagents.

Experimental

Materials

Table 1 contains detailed assay materials and instrument imaging supplies used.

Table 1. Assay materials and instrument imaging supplies.

Category	Description/Source/Part Number
Model Organisms	
Pseudomonas aeruginosa GFP (PAGFP)	*Pseudomonas aeruginosa* GFP (ATCC; p/n 15692GFP)
Escherichia coli GFP (ECGGFP)	*Escherichia coli* GFP (ATCC; p/n 25922GFP)
Staphylococcus aureus (SA)	*Staphylococcus aureus* subsp. *aureus* Rosenbach (ATCC; p/n 25923)
Bacillus subtilis (BSub)	*Bacillus subtilis* subsp. *subtilis* (Ehrenberg) Cohn (ATCC; p/n 35021)
Staphylococcus epidermidis (SE)	*Staphylococcus epidermidis* (Winslow and Winslow) Evans (ATCC; p/n 12228)
Vessels	
96-well microplate	Corning clear polystyrene (PS) (Thermo Fisher Scientific; p/n 12-566-202)
96-well microplate	Agilent Black PS optically enhanced clear bottom; (p/n 204626)
96-well microplate	Krystal Black PS glass bottom (Southern Labware; p/n 324002)
96-well microplate	Nunc MaxiSorp clear F8 breakaway wells (Thermo Fisher Scientific; p/n 469957)
24-well microplate	Krystal Black PS glass bottom (Southern Labware; p/n 324042)
Agar plate	100 mm x 20 mm Style culture dish (Corning; p/n 430591)
Dual-lock culture tubes	14 mL (Falcon; p/n 352059)
2 mL microcentrifuge tubes	Screw cap (Fisher; p/n 02-682-558)
15 mL centrifuge tubes	Screw cap (Corning; p/n 430790)
Media and Reagents	
Tryptic soy broth (TSB)	Cell culture medium (BD; p/n 211825)
Agar	Bacterial isolation, viability, growth (Sigma-Aldrich; p/n A1296)
Ampicillin	Antibiotic/media additive fluorescence protein selection (Sigma-Aldrich; p/n A5354)
Glycerol	Bacteria preservative, media additive (Sigma-Aldrich; p/n G9012)
Glucose	Media additive (where noted) (Sigma-Aldrich; p/n G9012)
McFarland latex turbidity standards	Hardy Diagnostics (p/ns ML05; ML1; ML2; ML3; and ML4)
FilmTracer SYPRO Ruby biofilm matrix stain	Biofilm EPS stain (proteins) (Thermo Fisher Scientific; p/n F10318)
Invitrogen SYTO 64 red fluorescent nucleic acid stain	Bacterial cell stain (Thermo Fisher Scientific; p/n S11346)
Invitrogen Toto-1 iodide	eDNA stain (Thermo Fisher Scientific; p/n T3600)
Presto Blue HS	Cell viability reagent (Thermo Fisher Scientific; p/n P50200)
Propidium Iodide	Cell viability reagent (Thermo Fisher Scientific; p/n P3566)
FilmTracer LIVE/DEAD Biofilm Viability kit	Cell viability reagent (Thermo Fisher Scientific; p/n L10316)
Calcofluor white	Biofilm EPS stain (cellulose/polysaccharides) (Sigma-Aldrich; p/n 18909)
1% crystal violet	Biofilm total biomass (Sigma-Aldrich; p/n V5265)
Resorufin	Metabolic activity standard (AdooQ biosciences; p/n A21344)
DPBS or PBS	(Dulbecco's) Phosphate Buffered Saline (Sigma-Aldrich; p/n D8537) or (Thermo Fisher Scientific; p/n 14190-136)
Imaging Supplies—Objectives	**Part Number**
2.5x Meiji Plan Apochromat	1220549
20x Olympus Plan Fluorite	1220517
60x Olympus Plan Fluorite	1220545
Imaging Supplies—Filters	**Part Number**
CY5	1225105
DAPI	1225100
GFP	1225101
Phycoerythrin (PE)	1225113
DAPI Confocal	1945103
GFP Confocal	1945104
TRITC Confocal	1945106

Methods

See references 5, 9, 10, 15, 23, and 25-29 for context and frameworks of many of the techniques, analysis, and methods adapted and defined in this study. Image acquisition and analysis details are provided in Table 2.

Cell culture

Working stocks of model organisms were prepared in tryptic soy broth, supplemented with 10% glycerol and filter-sterilized ampicillin, at 300 µg/mL for PAGFP, or 100 µg/mL for ECGFP. Glycerol working stocks were kept at –80 °C. Culture media was TSB supplemented with or without strain-specific ampicillin. Tryptic soy agar (TSA) was prepared by adding agar at a 1.5% (w/v) to TSB. Strain-specific ampicillin was added when TSA cooled to between 49 and 55 °C following autoclaving. Bacteria were isolated, grown, and cultured following one of two methods: (A) In the first method, a loop of working stock was streaked on strain-specific TSA and colonized at 37 °C. The next day, one to two isolated colonies were suspended in 6 mL strain-specific TSB in Falcon tubes, and were grown aerobically for 16 to 24 hours at 37 °C with agitation at 180 rpm on a Thermo Fisher Scientific MAXQ 4450 benchtop orbital shaker to obtain a final bacterial culture. (B) In the second method, a loop of working stock was suspended directly into 6 mL strain-specific TSB, then grow aerobically at 37 °C with shaking at 180 rpm for 16 to 24 hours.

Cell density calibration

Three 200 µL replicates of each McFarland latex turbidity standard, DPBS, water, TSB, and/or 95% ethanol were dispensed into a 96-well Corning or Agilent microplate and read at an optical density (OD) of 625 nm to obtain a final turbidity calibration curve, plotted using linear regression. The mean of the DPBS, water, media, and ethanol were calculated as the zero standard. Limit of blank (LoB) and limit of detection (LoD) for 32 replicates of 200 µL of DPBS were calculated using the parametric option described by the Clinical Laboratory Standards Institute EP17-A2 standard.[2] The calibration curve experiment file was subsequently used in all experiments to determine both starting overnight growth density and starting experimental cell densities following dilution of the overnight stock.

Cell seeding

Two 500 µL aliquots of overnight bacterial culture were set aside on ice to pause growth, and bacterial cell density was determined on the remaining overnight growth suspension by centrifuging at 6,000 *g* for 10 minutes in 2 mL tubes or at 5,000 *g* for 5 minutes in 15 mL tubes then resuspended in 5 mL DPBS. A seven-log serial dilution series was performed in DPBS, resulting in a final eight-log serial dilution series. Three replicates of 200 µL of each bacterial dilution were dispensed to a 96-well Corning microplate and the plate was read at an OD of 625 nm using the same calibration detection experiment file described above. The 500 µL aliquots of starting bacterial growth suspension were then adjusted to final density based on the results extrapolated from the McFarland standard curve by centrifuging, removing supernatant, and resuspending the bacteria in fresh TSB. Experimental seeding densities were generally diluted to a final ~ 1.5 to 3 x 10^5/mL.

Cell viability

0.047 grams of magnesium chloride ($MgCl_2$) was dissolved in 5 mL dH_2O to make a 100 mM starting stock solution. PAGFP TSB media (TSB + 300 µg/mL ampicillin) was supplemented with 100 mM $MgCl_2$ at final 0, 1, and 10 mM media solutions. A loop of PAGFP glycerol stock was resuspended in 6 mL of each of the media solutions and grown aerobically overnight at 35 °C with shaking at 180 rpm. The next day, the 0 mM overnight growth stock was divided into three 2 mL aliquots. One aliquot was designated for the air-liquid interface adherence assay (described later), and the remaining two aliquots were designated to test for viability of cells grown in the different media.

Metabolic viability was determined by interpolating samples from a resorufin calibration curve prepared in low-light conditions from a 1 mg/mL starting stock of resorufin in DMSO. A seven-point 2x dilution from 5 to 0 µg/mL resorufin in 95% ethanol was dispensed at 200 µL/well in triplicate to a black-sided 96-well microplate, and read kinetically every 10 minutes for 2 hours using fluorescence detection at Ex:Em 550:590 nm. A standard curve was generated for each time point using a nonlinear, four-parameter regression analysis. Data from the 30-minute time point was used as the final standard curve. Metabolic viability of samples was determined by plating 180 µL of a three-log dilution in triplicate for each of the $MgCl_2$ media formulations to a black-sided, clear-bottom 96-well microplate. A 20 µL volume of Presto Blue HS—a resazurin-based reagent—was dispensed to each well and read kinetically at 10-minute intervals up to 40 minutes using fluorescence detection at Ex:Em 550:590 nm. Concentration of sample resorufin for the 30-minute read point was interpolated from the resorufin standard curve.

Membrane viability of each $MgCl_2$ dilution of the overnight stock was determined using a live/dead assay[20] with some modifications. A 15 µL volume of a 20 mM solution of propidium iodide (PI) in DMSO was suspended in 5 mL dH_2O and kept in the dark. An 18-month stock of PAGFP, which had been kept in oxygen-starved conditions in stale media at 4 °C and was determined to be nonviable, was used as the dead cell control. The 0 mM overnight PAGFP growth stock was used as the live cell control. The turbidity of the dead cell control was determined from 200 µL stock solution, then centrifuged and resuspended in 1x balanced saline. The

live cell control was diluted to the same cell density as the nonviable stock by diluting the three-log dilution of the 0 mM stock 2.5x in balanced saline.

A live/dead standard curve was calibrated as a 100, 90, 50, 10, and 0% volume of live cells to the reverse of dead cells. A three-log dilution of each of the $MgCl_2$ samples was prepared in balanced saline. A 100 µL volume of each standard and sample were dispensed in triplicate into the inside wells of a 96-well black-sided, clear-bottom microplate. A 100 µL volume of balanced saline was dispensed to three wells as a no-cell control. A 100 µL volume of the PI solution was added to all wells and the plate was incubated in the dark at room temperature for 15 minutes. The plate was then read using fluorescence detection at Ex:Em 485:530 nm for live cells (green GFP), and at Ex:Em 485:630 nm for dead cells (red, PI). A ratio of the fluorescence emission values for all wells was calculated by dividing the green by the red emission value. Ratio values for the standards were multiplied by the dilution factor (2.5) to normalize standards to sample cell density. Ratio values were then plotted against percent live cells. Percent live cells for the sample ratio values were interpolated from the standard curve. To account for sample values interpolated as > 100% live, ratio values were plotted for each of the $MgCl_2$ concentrations against the ratio values of the 100% live standard (0 mM overnight growth stock).

Total biomass

A 200 µL volume of ~ 1.5 to 3 x 10^5/mL TSB suspensions of PAGFP, ECGFP, SA, and SE bacterial cells were dispensed in triplicate to four sets of Nunc breakaway wells. Each set of bacterial inoculum (time 0) was incubated at 37 °C at intervals of 3, 6, 16, or 24 hours. Total biomass of formed biofilms at each time point was detected in triplicate for each species using a crystal violet assay. Briefly, media were aspirated from the wells, and the well was washed twice with 200 µL DPBS and allowed to dry at room temperature with the lid off in a biosafety cabinet (≥ 30 minutes). A 200 µL volume of 99% ethanol was added to each well, and biofilms were fixed and permeabilized for 15 minutes at room temperature. Ethanol was aspirated and wells were allowed to dry completely (≥ 30 minutes). A 1% bulk crystal violet solution was diluted to 0.1% in dH_2O. A 200 µL volume of 0.1% crystal violet solution was dispensed to each well, followed by a 15-minute incubation at room temperature. Stain was aspirated and wells were washed twice with 200 µL sterile water, leaving the wells empty following the last wash. Wells were left to dry for at least 30 minutes. Stain was eluted from the biomass using 200 µL per well of 99% ethanol and shaking at 125 rpm for 30 minutes. A 200 µL volume of ethanol was dispensed into three wells as a negative control and total biomass on the plate was then detected, unless noted, at absorbance 590 nm. Biomass over time for each species was plotted against both the starting inoculation density before dilution and the mean crystal violet value.

Susceptibility

A 100 µL volume of diluted BSub cells (~ 1.5 x 10^5/mL) were resuspended in 1x TSB containing ± 150 µg/mL ampicillin and dispensed in triplicate into wells containing 100 µL of the same media (final cell density of ~ 0.75 x 10^5/mL). Cell growth with and without antibiotic was analyzed over an 18-hour kinetic time course reading turbidity at 625 nm absorbance every 30 minutes. In parallel, 100 µL cells ± 150 µg/mL antibiotic were dispensed in triplicate to Nunc breakaway wells into 100 µL of corresponding TSB (final cell density ~ 0.75 x 10^5/mL). The plate was incubated at 32 °C for 48 hours followed by a crystal violet assay (described previously) up to the elution step. Wells were left to dry overnight then imaged at 2.5x in color brightfield. The crystal violet elution step was then performed, and the plate was read at 590 nm OD. Biofilms were analyzed to compare growth and total biomass of antibiotic- and nonantibiotic-treated cells using turbidity at absorbance 625 nm and total biomass at 590 nm OD from the crystal violet assay. Qualitative assessment of total biomass was provided by the color brightfield widefield images.

Adherence—air-liquid interface

Seven replicates of 250 µL of a five-log dilution (~ 1.5 to 3 x 10^5/mL) of each of a 0, 1, and 10 mM $MgCl_2$ cultured overnight stock (described by the cell viability assay) were dispensed into 21 wells of two glass-bottom 24-well plates, one lying flat and the second propped at a 45° angle against a plastic block. Duplicate wells of the same volume of TSB without bacteria, and a single well of dH_2O, were also dispensed to each plate. Plates were incubated at 35 °C for 24 hours in the middle rack of the incubator either at a 45° angle or flat to the incubator tray insert. Spent media and nonadhered and loosely adhered cells were aspirated from all wells and replaced with 250 µL of respective fresh $MgCl_2$ supplemented media, then incubated either at a 45° angle or flat for another 36 hours to continue biofilm formation. Wells were washed with 250 µL PBS, then an additional 250 µL PBS was added to the wells and a 3 x 3 image montage was acquired at 2.5x in widefield, using a GFP filter to capture cell mass. To confirm cell mass, a single 20x, 40x, and 60x image in addition to acquisition of a 20x Z-stack in GFP was performed on one area of interest along the border of the visible biofilm (not shown). Biofilms were then fixed and permeabilized in 250 µL of 99% ethanol for 15 minutes. The remaining protocol for the crystal violet assay was performed as described by the total biomass assay up to the point

before elution. Plates were left to dry overnight then imaged using widefield color brightfield to capture total biomass at 2.5x in a 3 x 3 montage. The crystal violet assay was then continued through the elution step and detected at 590 nm OD. Finally, stain was aspirated from all wells, washed with sterile water until the residue was clear, then imaged again in a 3 x 3 montage at 2.5x using color brightfield and Cy5 to capture residual biomass staining. Image analysis comparing results of the plate grown at a 45° angle to the one grown flat was done for total intensity and area of cell mass (GFP) and OD of total biomass.

Adherence—surface affinity

A 5 µL volume of a ~ 1.5 to 3 x 10^6/mL suspension of SA was dispensed to 18-well quadrants of both a glass-bottom and optically enhanced polystyrene microplate and incubated at 37 °C for 3 hours. Three additional inoculations of 5 µL were added to the first at 2-hour intervals. At the end of the third incubation, 80 µL media was added to each inoculated well and the plates were incubated for an additional 16 to 24 hours. A 100 µL volume of media was dispensed to wells in rows D and H prior to the overnight incubation. For this experiment, overnight media was replenished with 100 µL fresh media every 16 to 24 hours over 8 days. On day 8, biofilms were imaged both before and after media replenishment. For unperturbed SA biofilms, 10 µL of 100 µM Syto 64, prepared in saline from an intermediary 5 mM concentration in DMSO, was added directly to the SA in growth media, and perturbed cells were aspirated normally and replenished with fresh media containing ± 10 µM Syto 64. Biofilms were then imaged at 2.5x using fluorescence to capture cell mass (TRITC). Analysis included comparing growth of the unperturbed biofilm to growth retained on perturbed biofilms for both microplate surfaces using the confluence calculation within the Agilent BioTek Gen5 Image Prime software. Briefly, percent confluence was calculated for each of the nine replicates of unperturbed and perturbed biofilms. The percent confluence of the perturbed biofilms was divided by the confluence values of the unperturbed biofilms and multiplied by 100, resulting in a percent retained growth end point.

EPS components and biofilm architecture

A 5 µL volume of a ~ 1.5 to 3 x 10^6/mL suspension of SA or ECGFP was dispensed to 18-well quadrants of both a glass-bottom and optically enhanced polystyrene microplate and incubated at 37 °C for 3 hours. Two additional inoculations of 5 µL were added at 3-hour intervals before adding a final 85 µL fresh media to each well and incubating for 16 to 24 hours. Wells in rows D and H were inoculated with 100 µL media only. For this experiment, 18 biofilm wells were assessed at each of three time points over a total of 3 days, and again at day 8. At each time point, Syto 64 at a final concentration of 10 µM/well and Toto-1 at a final concentration of 2 µM/well were dispensed directly to the SA wells and left to incubate for 15 minutes before adding one "drop" (~ 10 µL) of calcofluor white directly preceding the imaging step. For ECGFP-inoculated wells overnight, media was aspirated and replaced with 100 µL Ruby red matrix stain for 30 minutes at room temperature. The stain was aspirated, replaced with 50 µL of 1x calcofluor white for 1 minute, and then 50 µL sterile water was added and the wells were imaged. For remaining wells on the plate, spent media was exchanged with 100 µL fresh TSB and plates were returned to the incubator until the next time point. After the image analysis on the third time point, fresh media was replaced in remaining wells every 24 hours up to day 8, when the staining assay was repeated. This was done either using the staining method from previous time points on nine wells, or direct staining into the media without aspiration using 10 µL of 1x Ruby red biofilm stain and 10 µL of 1x calcofluor white for ECGFP, or using 10 µM/well of Syto 64, 2 µm/well Toto-1, and ~ 10 µL calcofluor white determined from an independent optimization experiment for direct staining. A Z-stack was acquired in confocal mode at 20x at 4.2 µm intervals over 13 stacks for SA and 25 stacks for ECGFP using the DAPI (calcofluor white), GFP (ECGFP and Toto-1), and TRITC (Syto 64) filter cubes. The Ruby red matrix stain was imaged in parallel to the confocal imaging at 20x in widefield using a phycoerythrin (PE) filter cube with excitation and emission spectrum (Ex:Em 469:593 nm) not available in confocal mode. Intracellular DNA (iDNA) and extracellular DNA (eDNA) were quantitated for SA biofilms, and microcolony growth was quantitated for ECGFP biofilms using cell analysis object counting and subpopulation metrics as defined by Table 2 and described in the "Results and discussion" section. Qualitative assessment for each of SA and ECGFP biofilm composition was compared on representative wells from each time point.

Instrumentation and software

All data was obtained using the Agilent BioTek Cytation 10 confocal imaging reader, equipped with programmable quad monochromators for absorbance and fluorescence detection, luminescence detection (not used), widefield inverted imager, and confocal inverted imager. The instrument was controlled by Gen5 Image Prime software version 3.12 or higher. Descriptions and the configuration of the detection and imaging supplies and acquisition settings are shown by Tables 1 and 2. Results analysis used either the Agilent BioTek Gen5 Image Prime software, Microsoft Excel for Microsoft 365 MSO (version 2208, build 16.0.15601.20540), and/or GraphPad Prism software, version 9.5.1 (733).

Table 2. Image acquisition and analysis settings. See Table 1 for imaging supply descriptions.

Assay	Imaging Mode	Imaging Method	Image Acquisition	Image Processing	Image Analysis (Parameters)
Properties					
Susceptibility	Widefield	Color brightfield	96-well plate; 2.5x objective autofocus height 2784.1 µm		Qualitative
Surffface Affinity	Widefield	Fluorescence	96-well single image; TRITC 556:600; 2.5x objective focal height 3000; LED intensity 10; Camera gain 32; integration 207 ms	Background flattening rolling ball 1132 µm	Image statistics (confluence; lower threshold 2000)
Air-liquid Interface	Widefield	Fluorescence	24-well plate 3 x 3 montage; GFP 469:525; 2.5x objective focal height 3000; LED intensity 10; camera gain 32; integration 780 ms	Image stitching linear blend; Background flattening rolling ball 6000 µm	Image statistics (total area; total intensity; lower threshold 5500)
		Color brightfield	24-well plate 3 x 3 montage; 2.5x objective focal height 3140.8	Image Stitching Linear Blend	Qualitative
Composition					
SA Biofilms, Global	Confocal 40 µm spinning disk	Fluorescence	96-well 20x objective Z-stack with interval 4.2 µm; GFP (green) 472:520; DAPI (blue) 405:442; TRITC (red) 556:600	ZProjection maximum method of in-focus stacks	Qualitative: Cell analysis (cell count eDNA, cell count iDNA, cell count colocalized eDNA–iDNA, cell count colocalized iDNA–eDNA. On total in-focus stack Z-projection days 1–3, on total and individual in-focus stacks day 8. eDNA strand analysis Day 3)
Day 1			15 Z-stacks; two slices below focal height; focal height red and green 3000 µm; integration times red 125, green 625; gain red 31.2, green 31.9	ZProjection red and green stacks 3–15; background flattening red and green 3 µm	Cell analysis (eDNA count green threshold 7750 object size 0.6–7 µm, subpopulation colocalized red mean ≥ 12000 *and* ≤ 38321; iDNA count red threshold 12000 object size 0.6–5 µm, subpopulation colocalized green mean ≥ 7750 *and* ≤ 50000)
Day 2			28 Z-stacks; one stack below focal height; focal height 3000 µm; integration times: blue 700, green 4000, red 2175; gain: blue 31.9, green 32, red 32	ZProjection stacks 16–20; background flattening rolling ball blue 126 µm, green and red 3 µm	Cell analysis (total eDNA objects and eDNA strand objects: GFP threshold value 5000, object size 1.2–11, subpopulation analysis objects size ≥ 2.2 *and* circularity ≤ 0.25, subpopulation colocalized red mean ≥12000 *and* ≤ 40000)
Day 3			50 Z-stacks; 10 images below focal height; focal height 3000 µm; integration times blue 1675, green 875, red 75; gain blue 32, green 31.9, red 30	ZProjection stacks 14–50; background flattening rolling ball green and red 3 µm	Cell analysis (total eDNA objects threshold 7750, object size 0.6–7, subpopulation co-localized objects red ≥ 12000 *and* ≤ 38321. Total iDNA objects threshold 12000, size 0.6–5, subpopulation colocalized green objects ≥ 7750 *and* ≤ 50000)
Day 8			13 Z-stacks, focal height 3,000 µm	ZProjection stacks 9–13, and on 7–13. Background flattening green and red 3 µm	Cell analysis (eDNA green threshold 7000, size 1-10, subpopulation colocalized red objects ≥ 5000. iDNA red threshold 5500, size 0.6–5, subpopulation colocalized green objects ≥ 8190)
ECGFP Biofilms, Global	Confocal, 40 µm spinning disk	Fluorescence	96-well 20x objective Z-stack with interval 4.2 µm; GFP (green) 472:520; DAPI (blue) 405:442	ZProjection maximum method of in-focus stacks	Qualitative: Cell analysis (microcolony enumeration)
	Widefield	Fluorescence	PE (red) 469:593 20x objective Z-stack with interval 4.2 µm		
Day 1			25 Z-stacks, one image below focal height, focal height 3086.9 µm; integration time green 4000, blue 100, red 2125; gains green 32, blue 32, red 32	ZProjection stacks 1–25, background flattening green 1 µm fine results, blue 126 µm red 10 µm fine results	Qualitative
Day 2			28 Z-stacks, two images below focal height, focal height 3000 µm; integration time green 4000, blue 75, red 128; gains green 32, blue 31.1, red 32; illumination red 10	ZProjection stacks 1–28, background flattening green 1 µm fine results, blue 25 µm red 126 µm	Qualitative
Day 3			50 Z-stacks, 10 images below focal height, focal height 3000 µm; integration time green 1025, blue 150, red 107; gains green 32, blue 31.2, red 32; illumination red 10	ZProjection stacks 1–50, background flattening green 1 µm fine results, blue 12 µm fast speed red 12 µm fast speed	Qualitative
Day 8			36 Z-stacks; focal height 3000 µm; integration times blue 250, green 150, red 6; gain blue 31.4, green 31.7, red 31.7; illumination red 10	ZProjection stacks 7–17 and stacks 7–13; background flattening rolling ball green 50 µm, red 60 µm	Qualitative: Cell analysis (individual cells green threshold 12000, size 0.8–11 µm. Cell colonies green threshold 8000, size 15–50 µm, subpopulation exclude colocalized protein ≤ 5000. Protein colonies red threshold 5000, size 15–50 µm, subpopulation exclude colocalized cells ≤ 8000)

Results and discussion

Cell density and total biomass—UV-Vis absorbance detection

The Cytation C10 is equipped with a custom-programmable UV-Vis absorbance quad monochromator, allowing the ability to tailor absorbance measurements over a range of 233 to 999 nm. This was useful in calibrating a cell density method using turbidity, for measuring relative total biomass of biofilms using a crystal violet assay, and for monitoring planktonic bacteria susceptibility to antibiotic over time. Representative results are discussed below and shown in Figures 2A to 2D and 5D.

Measuring turbidity of a bacterial suspension is a standard method for determining the cell density of a sample in a reproducible way that can be applied across laboratories and instrument platforms capable of absorbance detection. An important part of this procedure is to calibrate absorbance values to cell density per mL. One way to achieve this is by calculating a standard curve using turbidity standards. The cell density of a sample can then be interpolated from the curve for any number of subsequent experiments. There are a few considerations for implementing this method, such as differences between absorbance detection system sensitivity, the influence of cell suspension volume in the well on optical density value, and the influence of size and morphology variation between species on turbidity. For example, larger bacterial cells, like BSub, would be expected to have a higher OD at the same density as smaller cells like SA. Additionally, SA is known to form clusters during culture and growth that even vortexing or shaking may not disperse. Therefore, some species may warrant results from an orthogonal method like a hemacytometer or colony counting on an agar plate to be calibrated back to OD. Although methods can be developed to work around this, such as using sonication to disrupt SA clusters, it is generally understood that the same turbidity result from an SA bacterial suspension represents a cell density that is more likely to be one log higher than reported for other species like *E. coli*. In the experiments performed in this study, final cell densities were potentially biased, as cell density calculations were not corrected for cell size or morphology.

An additional constraint of the turbidity method is found in relation to the limit of blank (LoB) and limit of detection (LoD) at the volumes and detection setting used. Although less susceptible to saturating absorbance values at the high end, turbidity is not a reliable method for verifying cell dilutions below those of the LoD—a value on the Cytation C10 found to be just above that of the zero standard on the turbidity standard curve, and just below the McFarland 0.5 standard (1.5 to 3 x 10^8/mL) at 200 µL. Having an accurate and reproducible determination of a starting density is therefore also important to increase confidence of subsequent dilutions that will result in ODs below the LoD value and may not be traceable below the LoB. The LoB and LoD can also introduce bias in lag times during kinetic bacterial growth monitoring, as registered ODs below those values, such as when using low starting seed densities, will not increase until the LoB threshold is met and exceeded within the cell suspensio,n even if the cells have started dividing. An example of the calculated turbidity standard curve used in these studies, including the LoB and LoD, and representative results for calculated values of a bacterial suspension, is shown in Figure 2A. An example of kinetic growth monitoring using absorbance is shown in Figure 2D.

Another common assay using absorbance detection is the crystal violet assay assessing total biomass of a biofilm. This assay is one of the most universally cited assays in biofilm publications due largely to its simplicity and a workflow allowing quick turnaround for high-throughput biofilm analysis. This assay was useful to screen distinct species for biofilm properties such as qualitative assessment of morphological characteristics when grown in a 96-well plate using a ring assay (Figure 2B) and quantitative assessment of biofilm growth over time (Figure 2C). Figure 2B reveals a distinct ring formation for PAGFP, indicative of a preference to grow where oxygen is readily available at the air-liquid interface. Figure 2C reveals prolific growth of PAGFP biofilm compared to other species, with little to no growth of SE. These results were expected as PAGFP is known to overexpress two polysaccharides that contribute to formation of a "pellicle" during biofilm formation. This factors into increased total biomass compared to non- or less-pellicle-forming species, and the strain of SE used in the experiment was chosen as a negative control as it is a known nonbiofilm-forming species.[12-14] Figure 2D presents turbidity and crystal violet absorbance data in concert with widefield color brightfield imaging for verifying antibiotic inhibition of BSub biofilm formation when exposed to 150 µg/mL ampicillin. Empirically, the primary limitations of the assay were found to be:

- It stains total attached biomass—a property that eliminates the potential to differentiate cell mass from other biofilm components and potentially stains extraneous substances that are not part of the biofilm.
- There are a number of aspirate and dispense steps in the assay that warrant care as biofilms can be disrupted, resulting in the elimination of final total biomass. These

steps also make the assay less compatible to biofilms formed as nonattached aggregates.

– The elution step of the assay should be optimized as residual dye may remain in dense and strongly adhered biofilm, resulting in higher variability and lower accuracy of results (see Figure 5E).

– The crystal violet stain has a very low saturation point when detected by absorbance, requiring dilution of some results to come within the detection sensitivity of the reader (OD ≤ 4.0).

Although diluting any given biomass at the end of an assay is relatively straightforward, it is an extra step, and the dilution factor should be applied to the absorbance value. Although this potentially increases the relativity of the result, as absorbance values on 1:10 dilutions of pure crystal violet in water were not linear (data not shown). One workaround lies in reading eluted crystal violet by fluorescence using the extended gain mode available in Gen5 Image Prime software to increase the range of detection. Regardless of these findings, the assay is suitable for any biofilm application, particularly as a biofilm screening method for species biofilm formation, treatment response, or as a comparative model for other quantitative procedures.

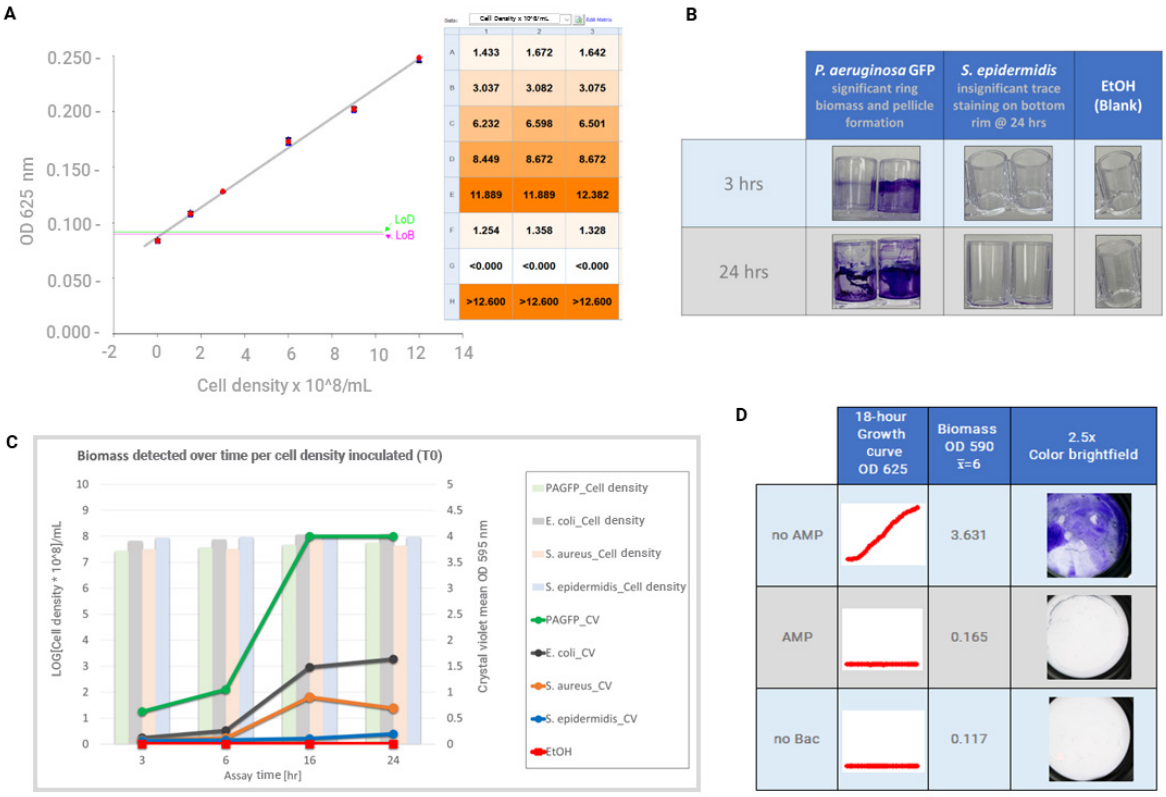

Figure 2. Examples of UV-Vis absorbance detection assays used in this biofilm evaluation. (A) Turbidity standard curve calculated to obtain cell density values for biofilm seeding dilutions showing LoB and LoD values. Example of calculated densities from the curve for a bacterial serial dilution is shown (right). (B) Qualitative assessment of biofilm growth at two time points for two of five species in (C) using the crystal violet assay. (C) Quantitative results of the crystal violet assay on biofilm growth of five bacterial species over time in relation to the inoculated cell density calculated from the turbidity standard curve. (D) Results using absorbance detection and widefield microscopy to assess susceptibility of BSub to the antibiotic ampicillin during planktonic growth and then following biofilm formation.

Cell viability—fluorescence detection mode

A common limitation generally reported about the use of fluorescence detection assays is that specific excitation and emission filters are required that provide the specificity and sensitivity for detection of a given fluorophore. The fluorescence detection module onboard the Cytation C10 has a variable-bandwidth quad monochromator from 9 to 50 nm in 1 nm increments and a wavelength range of 250 to 700 nm, allowing detection of a diverse range of fluorescent assays regardless of the excitation and emission limitations often found in filter-based systems. The fluorescence detection module was used in this evaluation to compare measures of cell fitness in overnight growth stock following exposure to different concentrations of a supplement within the culture media.

Assessing cell viability in starting biofilm cultures is important to gauge relative cell health of the culture and provide a basis for normalization of biofilm results in experiments that use viability as an end point to measure the effects of applied variables. In this case, an experiment was done to measure the viability of PAGFP planktonic cells after overnight growth in culture media supplemented with different concentrations of $MgCl_2$, before propagating the stock in a subsequent air-liquid interface assay. This was done to investigate the same on biofilm growth, as it has been shown that $MgCl_2$, in addition to acting in a concentration-dependent manner as a stimulant of bacterial cell division, is also reported to have antibacterial properties, potentially due to actions on the bacterial cell membrane.[22-24]

There are many cell viability fluorescent reagents that are amenable to bacterial cells. The advantage of these assays is that they are relatively inexpensive, widely available, reliable, and easy to perform. A combination of these assays on a single culture can also be useful to inform on both metabolic and cell membrane viability in parallel, as described here. Two viability assays were reviewed. The first assay was a direct mix-and-read reagent that measures relative aerobic respiration activity of cells via an intracellular resazurin to resorufin reduction, where higher relative fluorescence indicates more metabolically active cells. Results for this assay were obtained by first calculating a standard curve for resorufin. Resorufin is innately fluorescent and was detected using Ex:Em 550:590 nm. The resorufin concentration of samples was then interpolated from the standard curve.

A calibration protocol feature available in Gen5 Image Prime software allows a standard curve to be read and calculated on the first plate, and successive plates can be read that use the same curve to interpolate resorufin concentration of samples. Two considerations are worth noting: (A) As with all fluorescence detection assays, it is important to determine the gain value for the excitation and emission pair used for detection. Gen5 Image Prime software has different options for determining the gain value, and data collected for this assay used the gain returned for the high-resorufin standard to use on all subsequent reads. (B) The resazurin reagent is time sensitive, and although it can be detected within 10 minutes of addition, over longer periods of time, an increasing assay window between signal-to-noise values is reported.[21] In this experiment, RFU values were obtained for the standard curve at 10-minute intervals over a 40-minute kinetic time course. A curve and assay window were calculated for each time point. Although reliable data with similar signal-to-noise values resulted at each time point (data not shown), the time point equating to 30 minutes after plating was used for calibration, and sample interpolation was therefore also done using the same time point following addition of the resazurin reagent. Figure 3A shows the resorufin calibration curve that was used to interpolate resorufin concentrations of PAGFP exposed to different concentrations of $MgCl_2$ in the culture media. PAGFP cultured cells retained high metabolic activity regardless of $MgCl_2$ experimental dose, indicating that the salt did not result in loss of cell respiratory viability in overnight cultures of planktonic cells.

The second viability assay reports on relative permeability of the cell membrane using a dual-dye system, where both intact and membrane-permeable cells are targeted by one reagent (green RFU), while the second reagent displaces the first in membrane-permeable cells (red RFU). Each of the two dyes is detected with the same excitation but a different emission wavelength. A higher relative fluorescent ratio between the emission values indicates more viable cells with intact membranes in the culture compared to compromised cells.[21] The assay was adapted using total PAGFP expression from a 2.5x dilution of the PAGFP without $MgCl_2$ (0 mM) as the live cell control in place of the green dye.

An expired PAGFP cell culture in stale media that is kept as a nonviable control was used as the "dead" cell control and dispensed at an inverse percent to the live cells within each standard. A live/dead cell curve was calculated from the ratio between the green signal for live cells and the red emission signal for dead cells plotted against the percent live cells within each standard. Ratio values obtained from the standard curve were multiplied by the cell dilution factor to normalize results to the tested samples (a 2.5x dilution of the live cell control resulted in the same starting cell density as the dead cells). Figure 3C shows the live/dead curve, and Figure 3D shows the viability ratio results for four replicates of PAGFP from each concentration of $MgCl_2$ compared to the ratio of the 100% live cell standard. Results from the live/dead assay indicate that the growth culture exhibits $MgCl_2$ dose-dependent membrane competence, with the increase in viability likely due to the growth stimulant properties of the salt, as previously reported.[25] This would therefore increase the live cell population in those samples.

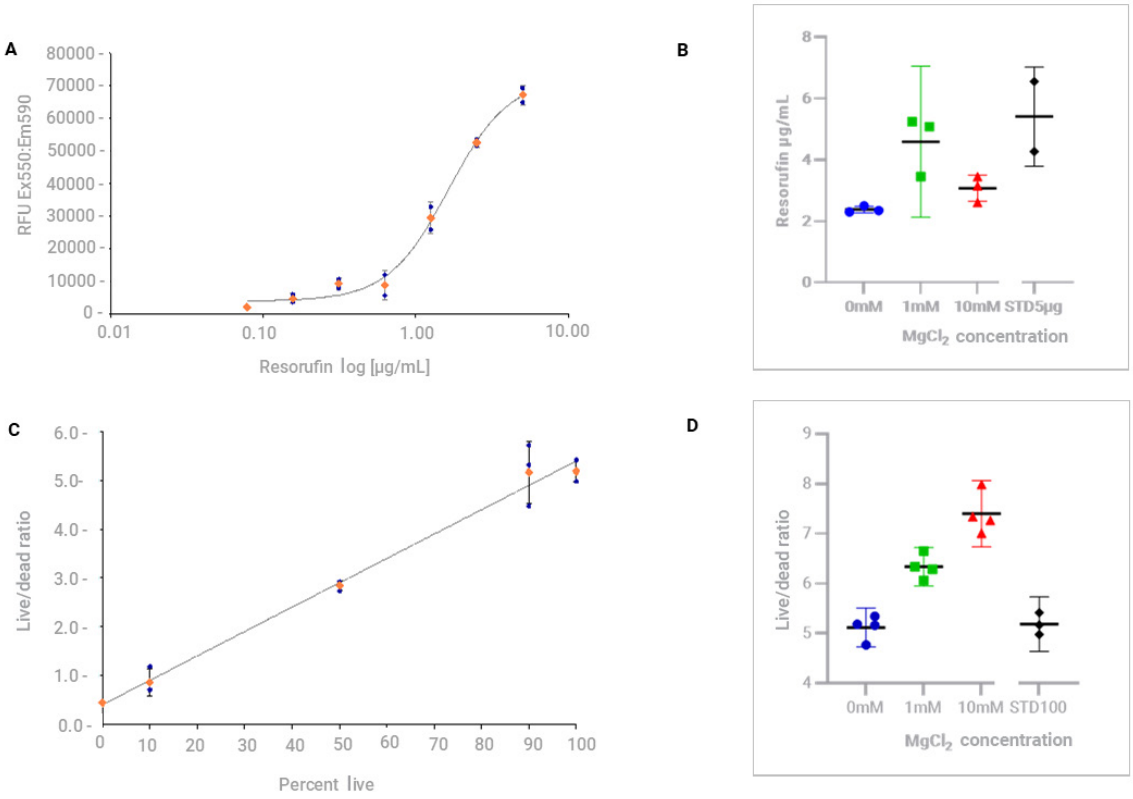

Figure 3. Examples of fluorescence detection assays used in this biofilm evaluation. (A) Resorufin standard curve, calculated to obtain metabolic viability values for biofilm seed stocks. (B) Resorufin concentration values interpolated from the standard curve to assess aerobic respiration activity of samples cultured with different concentrations of $MgCl_2^+$ in the growth media. (C) A live/dead assay standard curve, using the 0 mM $MgCl_2$ PAGFP bacteria stock as the live cells, and PAGFP cells from an expired lot as the dead cells. (D) Membrane competence of the same sample cells assessed in (B) compared to the 100% live cell standard (STD100) prepared from the 0 mM stock.

Adherence—color brightfield and fluorescence widefield microscopy

A recent study reported evidence that up to 80% of bacteria and archaea on Earth exist as biofilms.[7] Although relatively nondisruptive and even synergistic in an organic context, biofilms can also cause persistent disease and infection in natural systems and irreparable damage in inorganic environments. Technically, biofilms are defined as "an aggregate of microorganisms, like bacteria, in which cells are frequently embedded within a self-produced matrix of EPSs and adhere to each other and/or to a surface".[8] There is extensive science done to understand biofilm adherence properties, including:

- Mechanistic/molecular changes in the bacteria
- Variables influencing their preference for different surfaces or bacterial species
- The effects of environmental conditions on attachment
- Whether different surface or other treatments—either applied or integrated into an experimental surface directly, or to biofilms growing on a surface—can prevent, promote, or eliminate biofilm attachment.

Under circumstances where there can be numerous assay parameters to optimize, it is useful to have high-throughput screening methods that can efficiently produce data that is relevant to answering macro questions such as how much and/or what parts of a biofilm biomass may remain or be eliminated by experimental variables, where microanalysis of individual cells or biofilm constituents is less informative.

The widefield microscopy module on the Cytation C10 is a useful tool for performing high-throughput macroanalysis of biofilms. An entire well of a 96-well plate can be captured using a low-magnification 2.5x objective or, using a 3 x 3 image montage. A low-magnification 2.5x objective can capture an entire well of a 96-well plate in one image or, using a 3 x 3 image montage, each well of a 24-well plate. This can be accomplished within a single protocol that defines several imaging modes including brightfield and fluorescence. In addition to facilitating differentiation of individual components of a biofilm from the total biomass for example, this low-magnification widefield imaging technique also benefits from both fast image acquisition times, enabling high throughput screening of multiple variables in parallel, and efficient use of computer memory by decreasing storage requirements for saving images and data, that may result from screening different nutritional factors or growth techniques during biofilm development. An image statistic interface within Gen5 Image Prime software can be used to calculate numerous high-level metrics that can be useful for quantitating larger representations of biology, such as areas of attached cell mass. The low-magnification and image statistics screening technique is demonstrated here by two experiments.

One experiment compared biofilm surface affinity between two different microplates. The goal of the experiment was to investigate whether a less expensive bottom substrate designed for high-quality imaging (optically enhanced polystyrene (OEPS)) compared to a more costly one with a known high optical resolution (glass). This was done by evaluating cell mass confluence on both surfaces following perturbation from media aspiration in live biofilms. The variable of aspiration was chosen because it is a common occurrence in biofilm assay workflows, whether for media exchanges, staining, or washing of biofilms. The aspiration step can also challenge the use of automated liquid handling devices for biofilm assays, which in turn, can constrain the application of high-throughput workflows that are designed to reduce laboriousness and variability of manual methods. Representative wells of unperturbed and perturbed SA biofilms in Figure 4A are shown in a view highlighting cell mass confluence (red) using a threshold outlier feature (white) in image statistics. Gen5 Image Prime software calculates confluence in the Image Statistics interface as the number of pixels within a user-defined intensity range, divided by the total pixels of the image, multiplied by 100. The signal threshold defined for this experiment is shown in Table 2. In this experiment, cell confirmation within an area of the total cell mass was done using a 20x confocal image Z-stack, an example of this can be seen in the assay results represented by Figures 6 and 7. Using data from the mean of nine replicates of both aspirated and nonaspirated wells, Figure 4B indicates that, likely due to differences in ionic forces of the bottom surfaces, the glass surface resulted in statistically significant higher growth. However, the OEPS surface had a higher percent biofilm retention, indicating that cells may be more strongly adhered to the OEPS surface. Additionally, although both surfaces were subject to cell mass loss from gentle aspiration, irreversibly attached persister cells remained, and the biofilm was not entirely eliminated from either surface.

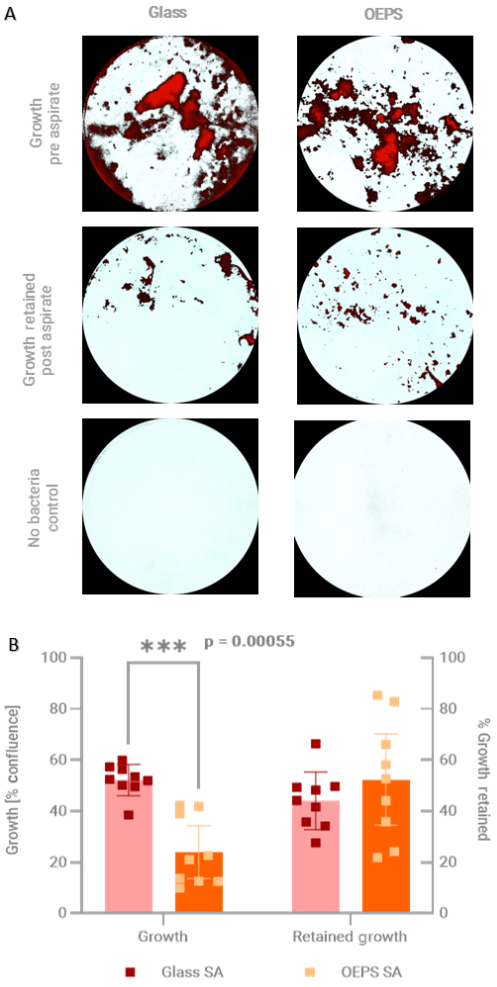

Figure 4. Widefield microscopy image analysis comparing SA biofilm surface affinity to different substrates. (A) Threshold images of live biofilm cell mass confluence on different surfaces before (growth) and after (retained) media aspiration on day 8 SA biofilms. (B) Biofilms grew more but retained less cell mass on glass than on the composite surface at day 8.

The goal of the second experiment was to find optimal conditions for growing biofilms on the bottom of a high-density vessel that could be more conducive to imaging by reducing or eliminating biofilm growing outside the focal range of the microscope, such as vertically along the sides of the wells. This followed evidence from prior experiments (see Figure 2B) showing that PAGFP preferred to grow as a biofilm at an oxygen-rich air-liquid interface. This can be seen by the prominent ring of biofilm around the microplate wells from where the top of the inoculum volume was in direct contact with oxygen, and along the sides of the wells where the pellicle drapes down as a function of media aspiration. This pattern renders much of the biology incompatible to microscopic analysis within the vessel. An additional problem had been found from empirical data collected by independent experiments revealing that, after dispensing small volumes of bacterial inoculum onto the bottom of several different microplates, a quick migratory response of the inoculum towards the sides of the well bottom that were in contact with the walls of the vessel occurred. An experiment was therefore designed to screen for conditions favorable to the adherence of cells to the bottom of a microplate that could be captured within the widefield imaging field of view of the Cytation C10 in a high-throughput manner, allowing multiple replicates of multiple conditions to be tested in parallel. Two techniques were investigated. The first was to grow biofilm at an angle, where the air-liquid interface was in direct contact with the bottom of the vessel, resulting in an area of biofilm that could be captured by inverted microscopy, and to compare results from that to biofilms grown in vessels lying flat. The second technique was to use different concentrations of $MgCl_2$ as a supplement in the culture media, as it has been reported that in addition to the antibacterial and bacterial growth stimulating properties of $MgCl_2$[23, 25], the salt has also been investigated in a species-, concentration-, and media composition-dependent manner for possible effects on bacterial attachment through electrostatic and physiology-dependent adherence processes.[23] This could possibly mitigate the migration pattern observed empirically by manipulating the ionic charge within the vessel, making the sides along the bottom of the well less attractive to the cells. The workflow of the assay was to first verify whether $MgCl_2$ influenced planktonic growth and cell viability. These results were discussed previously and shown in Figure 3. The same growth stock from the viability experiments was prepared in fresh $MgCl_2$-supplemented media and inoculated in replicates of seven to either the angled or flat air-liquid interface plates to also gauge the effects of $MgCl_2$ for each method.

Three metrics were used to compare the growth methods. For each well, cell mass within the biofilm was differentiated using fluorescence imaging of GFP at 2.5x in a 3 x 3 montage (Figure 5A). Image statistics was used to calculate total signal intensity and total area of the cell mass (Figures 5B and C). Complete image acquisition and analysis settings are defined in Table 2. Several signal threshold settings were evaluated. Higher threshold values resulted in targeting areas of high signal intensity of the biofilm cell mass representing greater cell density, whereas lower signal threshold values captured more overall cell mass within the biofilm, including areas that were less dense. As slight differences in the experimental variables may be detected more at the low end than the high—for example high cell mass would be detected even

at lower thresholds, but lower cell mass areas could be lost from calculation at higher thresholds—a lower value that was representative of more cell mass was used for data analysis. The data shows that the total area and intensity values correlate in both a growth method and dose-dependent manner, with the 10 mM $MgCl_2$ biofilms grown flat having statistically significantly more total intensity and area of cell mass than biofilms grown with no $MgCl_2$ either flat or at an angle. The 10 mM angle replicates were more variable and somewhat less dense than those grown flat, but also still higher in both area and intensity than cell mass grown at 0 mM $MgCl_2$; however, these replicates were not significantly different than any of the other methods. The lower *P* values for the total intensity comparisons could indicate that the cell mass was also denser for the 10 mM $MgCl_2$ replicates, indicating more strongly adhered cell mass. This would coincide with the finding that $MgCl_2$ stimulates cell division and, in this case, even as a biofilm phenotype.[25] Of note, the 1 mM $MgCl_2$ biofilms presented with spurious and inconclusive results requiring further study and were therefore left out of this analysis.

Following GFP imaging, the biofilms were stained with crystal violet to assess total biomass within the wells. Following fixation, staining, and drying overnight, the total biomass of each well was imaged at 2.5x as a 3 x 3 montage in color brightfield mode (Figure 5A). The crystal violet was then eluted as described previously and detected at 590 nm OD (Figure 5D). The two most notable results from the total biomass data were that the 10 mM flat replicates presented with lower overall total biomass than the 0 mM flat replicates, even though they had statistically higher total intensity and total area as calculated from the image analysis; and the 0 mM flat replicates were statistically different from both groups of replicates from the angle plates—findings also not supported by the image analysis. From past empirical data it was observed that residual crystal violet stain remained in biomass after elution and that this may be a cause of variability with the method. Following the detection step, therefore, stain was aspirated from the wells and the wells were washed until the liquid ran clear. The residual biomass was then dried, and the wells imaged again in color brightfield to capture any residual staining remaining in the well. Two examples of residual staining from the 0 mM angle and 0 mM flat plate are shown in Figure 5E (upper left and upper right of the quadrant respectively) compared to blank wells from the same plates. These biofilm wells were chosen because they were the furthest outliers from the crystal violet assay of each respective replicate set; both these replicate sets had the most significant variability and change from the cell mass data, and these replicate groups had the highest residual staining of all replicate groups as determined qualitatively. This may reinforce the previous findings that would suggest residual noneluted crystal violet may be a cause of increased variability in biofilms. Less residual staining in the 10 mM flat replicates, and a lower overall total biomass readout for those replicates than for the 0 mM flat plate, could indicate that the presence of $MgCl_2$ may result in less pellicle formation even with higher cell density, as has been previously reported.[25] This could also be supported by a qualitative assessment from the 10 mM angle representative well in Figure 5A that visually presents with thinner and lighter staining of the noncell mass areas of the total biomass where the pellicle would stain, as compared to the 0 mM angle well, for example.

In summary, the collective data suggest that PAGFP biofilms supplemented with 10 mM $MgCl_2$ and grown lying flat within a microplate vessel produced biofilms with higher cell mass, but potentially less pellicle formation in proportion, compared to those grown at an angle with or without supplement, or flat with no supplement. All methods resulted in robust biofilm formation containing high-density cell mass conducive to inverted imaging through the bottom of the vessel using a low-magnification, high-throughput approach. Image analysis proved a sufficient and enhanced method for screening data on individual components of a biofilm as represented by cell mass than the comparative crystal violet assay that does not discriminate individual biofilm components.

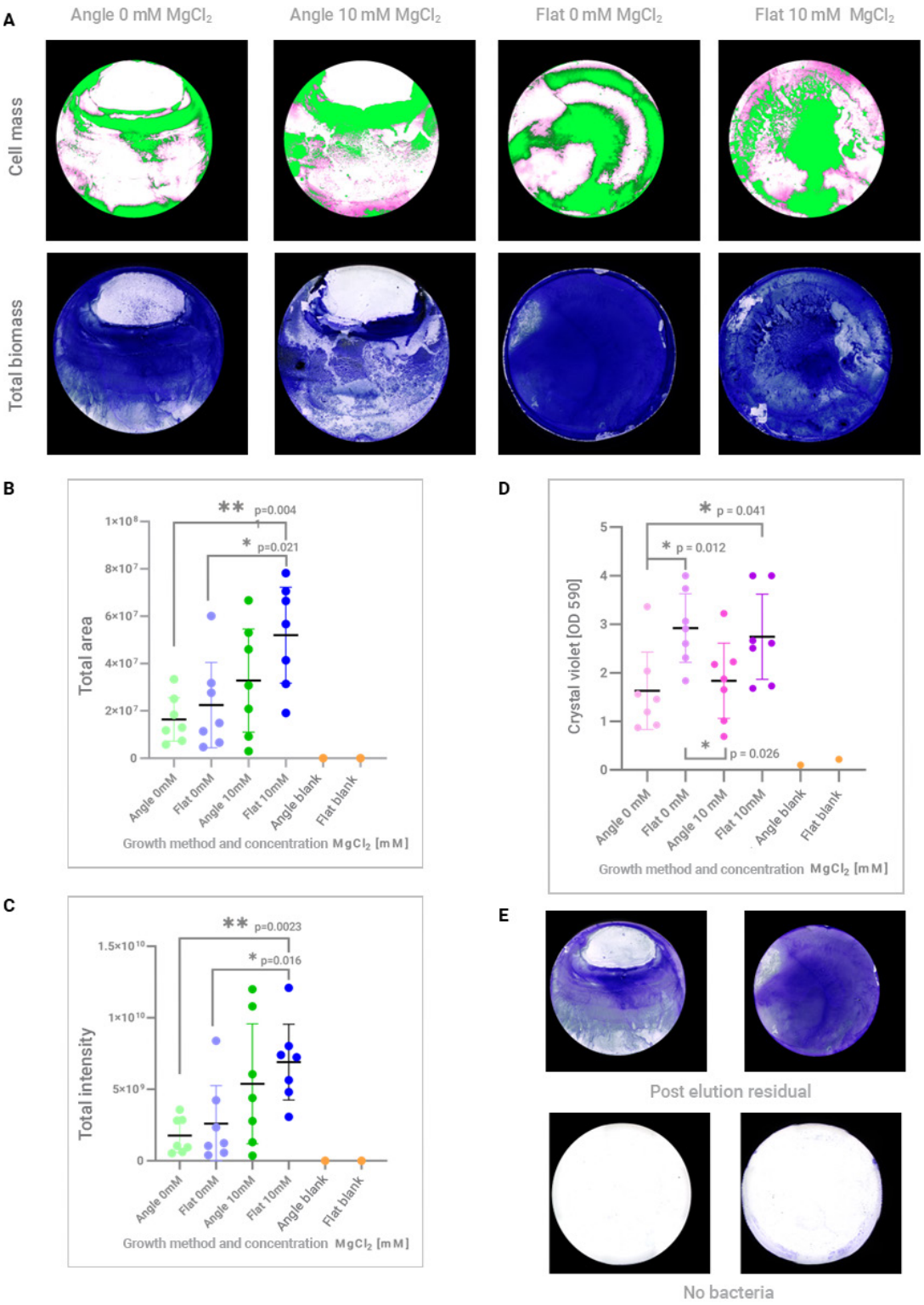

Figure 5. Widefield image analysis comparing PAGFP biofilm adherence using different growth methods and media concentrations of $MgCl_2$. (A) Images of biofilm cell mass in live biofilms and total biomass postfixation and crystal violet staining when grown flat or at a 45° contact angle to the bottom of a microplate with and without $MgCl_2$. (B) Total cell mass area for each condition. (C) Total cell mass signal intensity for each condition. (D) total biomass detected using absorbance detection of eluted crystal violet staining. (E) Examples of residual crystal violet staining after elution, demonstrating artifact of the method for a 0 mM angle (top left) and a 0 mM flat (top right) well compared to blank wells from the respective test plates (bottom). All error bars are the mean ± 95% confidence interval.

EPS components and architecture— confocal microscopy

Biofilms are characterized by the development of an EPS that is propagated when bacteria develop a biofilm lifestyle. This gives them an inherent three-dimensional quality that can be observed and reconstructed using optical sectioning with a confocal microscope. Although a widefield imager can also capture biofilm compositional properties, confocal laser scanning microscopy (CLSM) is frequently used in biofilm studies due to the ability to reduce out-of-focus light and improve image quality. The reduced background resulting from this method is especially useful when imaging live biofilms over a range of focal heights in host or experimental media, as background such as media autofluorescence can often interfere with acquiring clear images during more detailed microanalysis of very small objects such as bacteria or other biofilm components. This can become more pronounced when moving deeper into the biofilm volume.[9, 10, 15]

The Cytation C10 confocal imaging reader enables capture of fluorescent images across the blue to far-red spectrum with a choice of seven filter cubes and two spinning-disk sizes to accommodate both lower and higher magnification from 20 to 60x. The Gen5 Image Prime software Z-stacking tool can be defined for step intervals as low as 0.1 µm over a total stack height of up to 3,333 slices depending on interval step size. Numerous different stage adapters are available to accommodate a variety of labware vessels suitable for 3D image analysis of biofilms.

Two assays, one using a gram-positive and the other a gram-negative species, were performed to evaluate biofilm composition using the confocal microscope on the Cytation C10. In one assay, SA biofilms were used to monitor the presence and localization of eDNA in relationship to iDNA over time. eDNA is a key component of bacterial biofilm EPS with a role in biofilms that continues to be investigated, but has been shown to potentially represent a mechanism for horizontal gene transfer in bacteria and/or provide structural definition resulting in channels that enable moving, diffusing, and/or assimilating constituents within the biofilm, such as nutrients, waste, or therapeutics.[3, 4, 11, 16]

A lack of colocalization of eDNA and iDNA within the biofilm, in addition to the presence of both free eDNA strands and transitionary states of eDNA availability in the matrix following loss of cell viability, could represent support for the theories that eDNA plays both a structural role and gene transfer mechanism with SA biofilms. This hypothesis was investigated qualitatively and quantitatively using two nucleic acid stains that differ in their cell permeability to differentiate and determine colocalization of iDNA and eDNA. Polysaccharides within the biofilm EPS were visualized using a counterstain for cellulose.

Characteristics of an eight-day lifecycle of SA biofilms was assessed using qualitative analysis on optimal Z-stack images obtained from confocal microscopy at 20x. Results are shown in Figure 6.

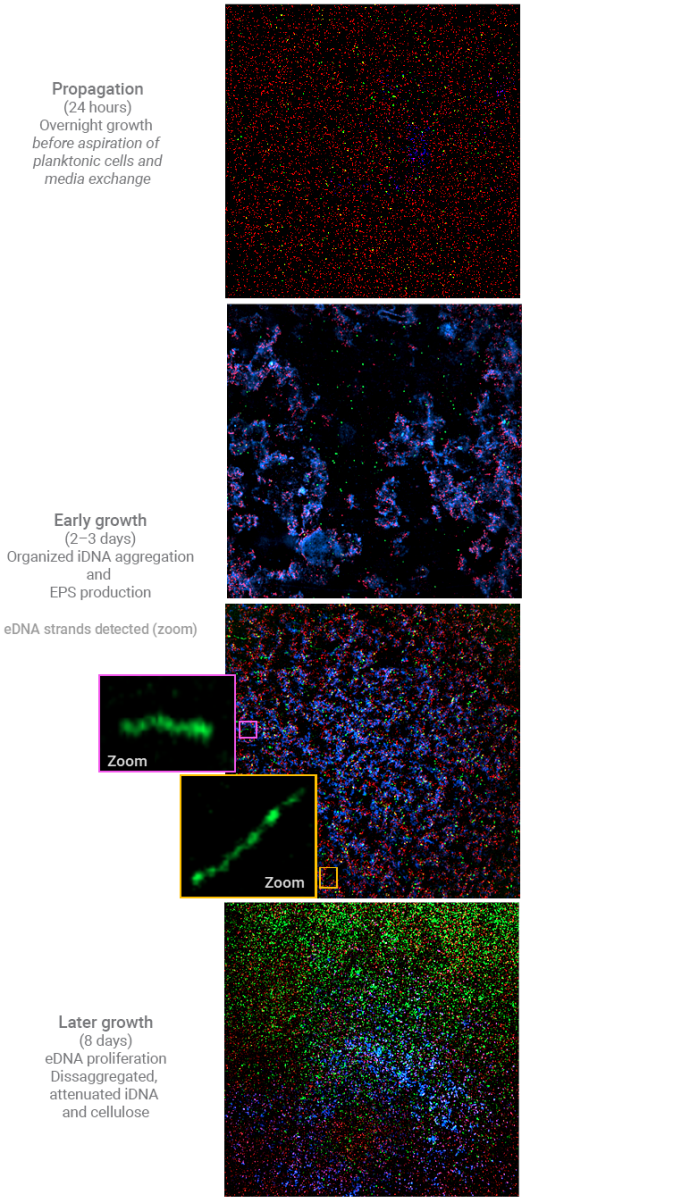

Figure 6. Qualitative assessment of SA biofilm development over time. iDNA (red), eDNA (green), polysaccharides (predominately cellulose, blue). Although most eDNA staining is due to membrane permeability of intact nonviable cells, examples of eDNA strands are highlighted in the early growth matrix (zoom insets). Images are taken from live biofilms.

Cell analysis was then used to compare percent eDNA, iDNA, and colocalized objects within the biofilm over the same time periods using multiple Z-stacks. The cell analysis steps taken to differentiate and quantitate the percent of eDNA, iDNA, and colocalized objects on each in-focus Z-stack compared to a Z-projection on all in-focus stacks is shown in Figure 7.

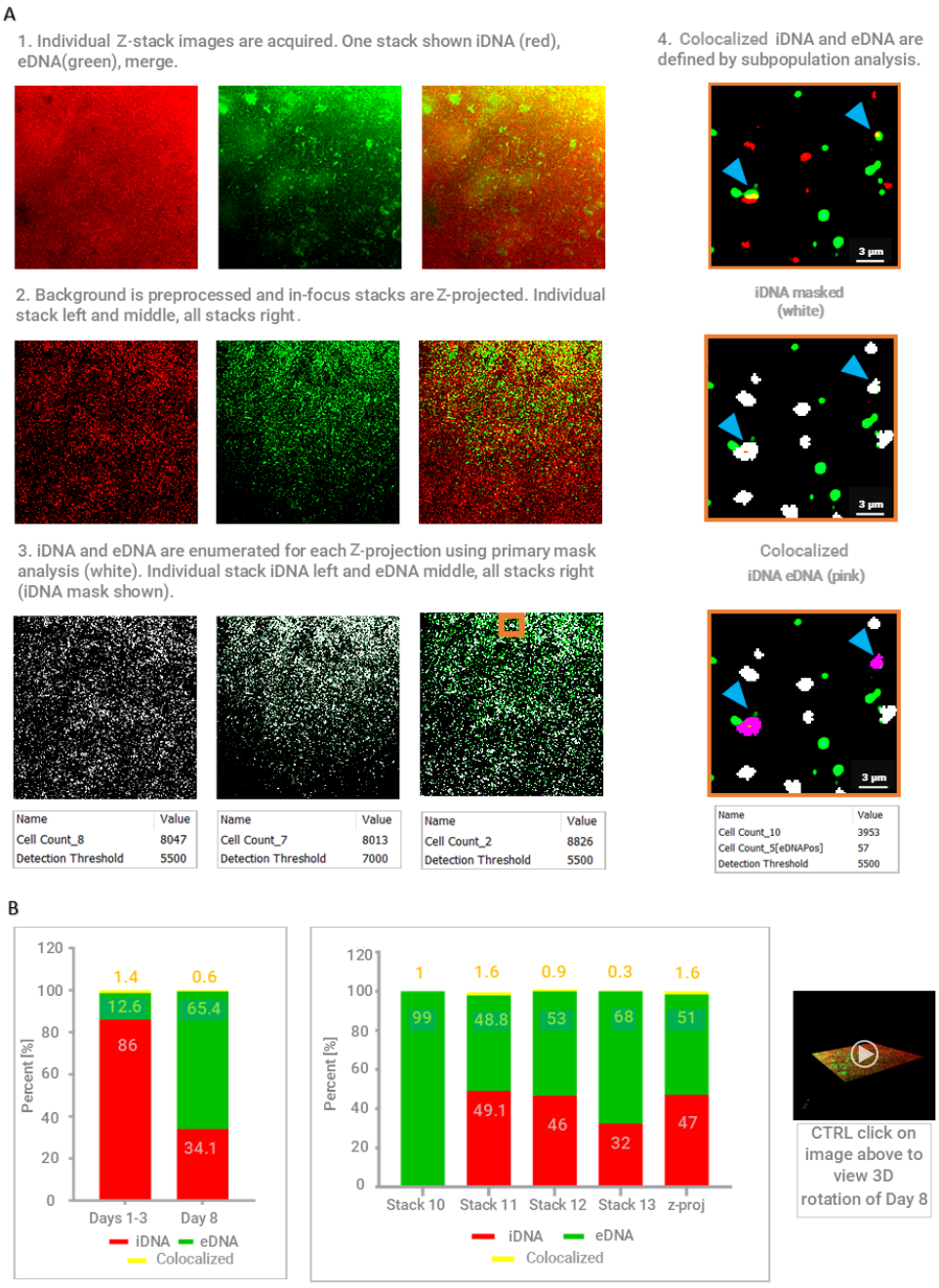

Figure 7. Quantitative analysis of eDNA and iDNA in live SA biofilms using the Agilent BioTek Cytation C10 confocal imaging reader and Gen5 Image Prime software confocal Z-stacking image analysis. (A) Steps for enumerating eDNA and iDNA in SA biofilms (left). Subpopulation analysis is used to define colocalized eDNA and iDNA objects (step 4, right). The orange border area in the step 3 image represents the zoomed imaged area in step 4. Blue arrows identify colocalized objects. (B) Percent of eDNA, iDNA, and colocalized objects calculated from total eDNA and iDNA objects are graphed. (Lower left) the mean percent is plotted on n = 6 from Z-projections of total in-focus stacks for each individual day. (Lower middle) Percent objects for each in-focus stack compared to the Z-projection of all stacks is shown for one day 8 biofilm. (Lower right) The thumbnail image accesses a rotating 3D rendition of stacks 10 to 13 represented by the middle graph.

The Z-projection comparative analysis containing all in-focus stacks was done based on a premise that iDNA and eDNA may be more likely to overlap in a compressed Z-plane then within any individual stack, a property of Z-projection on multiple stacks that could bias both the enumeration and localization of individual objects. A distinct geography of eDNA and iDNA within the biofilm was found from this analysis. The data from both the Z-projections of all in-focus stacks from all days and individual stack data extrapolated for day 8 shows a compelling lack of overlap (≤ 1.6%) between eDNA and iDNA in both individual and multistack Z-projections. Although this finding could be partially biased based on the choice of signal threshold defining a colocalized object, a possible interpretation could be that iDNA and eDNA objects remain in a sessile mode within the biofilm, adding architectural features such as structural support or, as reported, channels within the biofilm, for example. The data also show that an inverse relationship of iDNA to eDNA developed during growth of SA biofilms, as indicated by a five-time increase in percent eDNA and a 2.5x decrease of percent iDNA from days 1 to 3 to day 8. It could be inferred from this that bacteria may enter a prolonged stationary stage over time due to growth density or other stress that results in slow or no viable cell proliferation within the biofilm, parallel to a loss of sustainable viability of existing cells. The quantitative cell analysis also resulted in a finding that, although a majority of eDNA was represented as a homogenous population of membrane-permeable nonviable cells, a distinct population of eDNA objects could be characterized as eDNA strands, such as those shown in Figure 6. Size and shape qualities of these strands was applied to enumerate them using subpopulation analysis, and the percent of these objects compared to the total eDNA masked within the image was calculated using a scatter chart analysis.

Figure 8 represents an example of the subpopulation analysis for a 48-hour biofilm, resulting in a calculated 4.5% of total eDNA objects defined as eDNA strand objects at that growth time point.

In the second assay, qualitative and quantitative analysis using confocal microscopy was used to evaluate microcolony development in ECGFP biofilms over time. These well-defined aggregates of cells and other EPS components have been hypothesized to form due to cellular quorum sensing as a way of conserving energy and resources while supporting an environment favorable for producing progeny.[5, 6, 18, 19] Findings from the qualitative assessment are characterized in Figure 9, illustrating observed stages of microcolony growth over four time points shown at 20x, with 60x images of individual channels from a single Z-slice from another replicate at day 8 shown for comparison.

Figure 10 describes a process for quantitating microcolonies using cell analysis steps to differentiate cellular and EPS protein components and enumerate well-formed and proliferated microcolonies, over each layer of a Z-stack acquired from the minimum and maximum height of in-focus cellular and EPS protein objects, from day 8 of biofilm growth. From the images at this time point the in-focus microcolony biology covered a total Z-height of 37.8 µm (Z-stacks were acquired at 4.2 µm focal height intervals). The graph of enumerated microcolony objects for each stack indicates correlation of cell and EPS colocalization over all in-focus stacks. A movie from the bottom to top stacks of the microcolony analyzed provides a visual rendition of this. In addition to showing a change in cell density over the Z-height of the microcolonies, which corresponds to a peak of enumerated cellular aggregates in the middle four stacks of the Z-plane, dense cell aggregates exist even in less-populated stacks. This can also be seen in Figure 9 from an earlier time point characterizing colony division, where there are few cells in the surrounding biofilm but densely coalesced cells colocalized to protein aggregates.

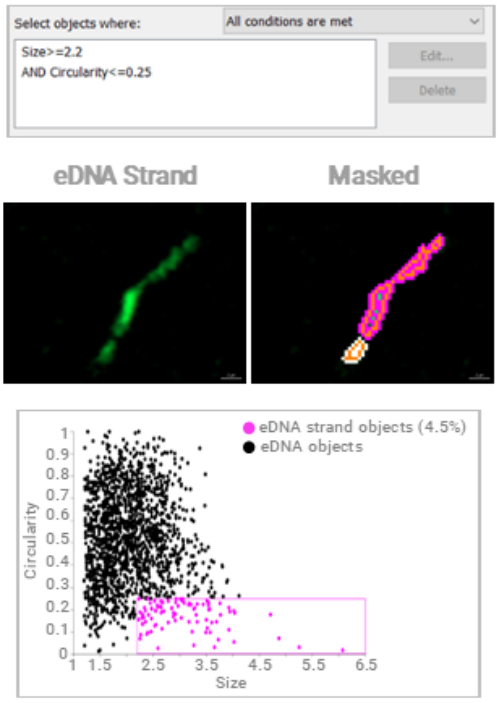

Figure 8. Subpopulation analysis of eDNA strand objects using the Agilent BioTek Gen5 Image Prime software. (Top) criteria for defining a subpopulation on eDNA strand objects; (center) example of eDNA object (left) identified by the subpopulation criteria with a pink mask (right); (bottom) scatter chart showing the percent of all objects meeting the subpopulation criteria in the image (pink) versus total eDNA objects enumerated (black). The full image for this representative data can be seen in Figure 6, shown with examples of other strand objects zoomed.

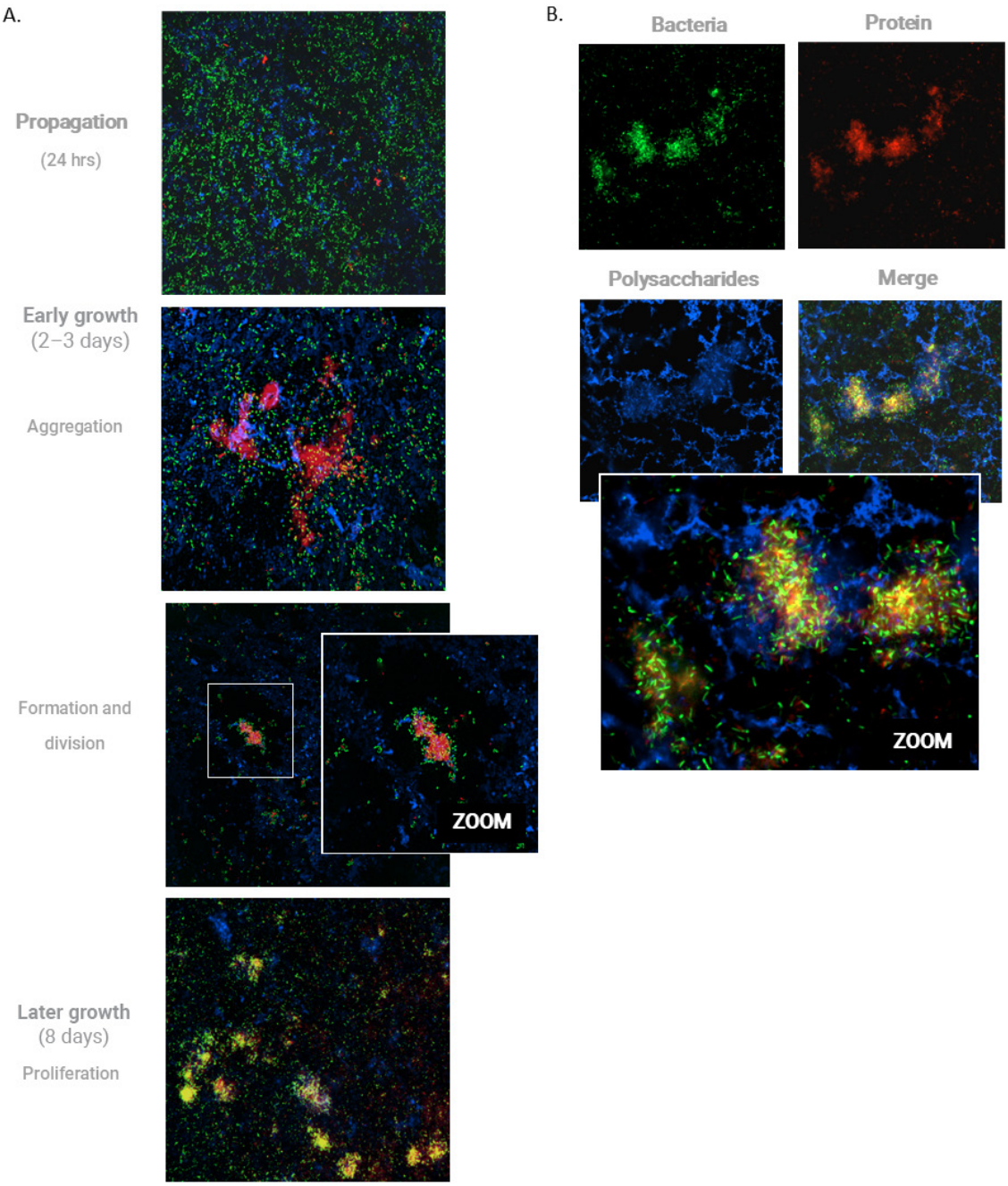

Figure 9. Qualitative assessment of ECGFP microcolony development in live biofilms. Bacteria (green), EPS proteins (red), EPS polysaccharides (predominately cellulose, blue). A) 20X evaluation over time. B) 60X at day 8 for comparison.

In contrast, protein aggregates remain uniformly enumerated over nine stacks, including the stacks with peak cellular aggregates, even continuing into higher elevation within the biofilm, where many of the protein aggregates (~15 out of 25) are no longer colocalized with cellular objects. Due to the number of microcolonies in the imaged area, one possible explanation for the increased individual cell density in some stacks may be the result of some microcolonies outside the imaged area collapsing and releasing progeny into the biofilm matrix. This, in turn, may lead to increased microcolony development, or more individual cells joining established microcolonies, for example. The finding that there are more protein aggregates more uniformly enumerated over the entire Z-plane, and prominently at the higher elevations where they no longer colocalize with cellular aggregates, could imply a structural scaffolding role for the proteins in microcolony development, acting as a cohesive element both layered with and enveloping the cells, for example.

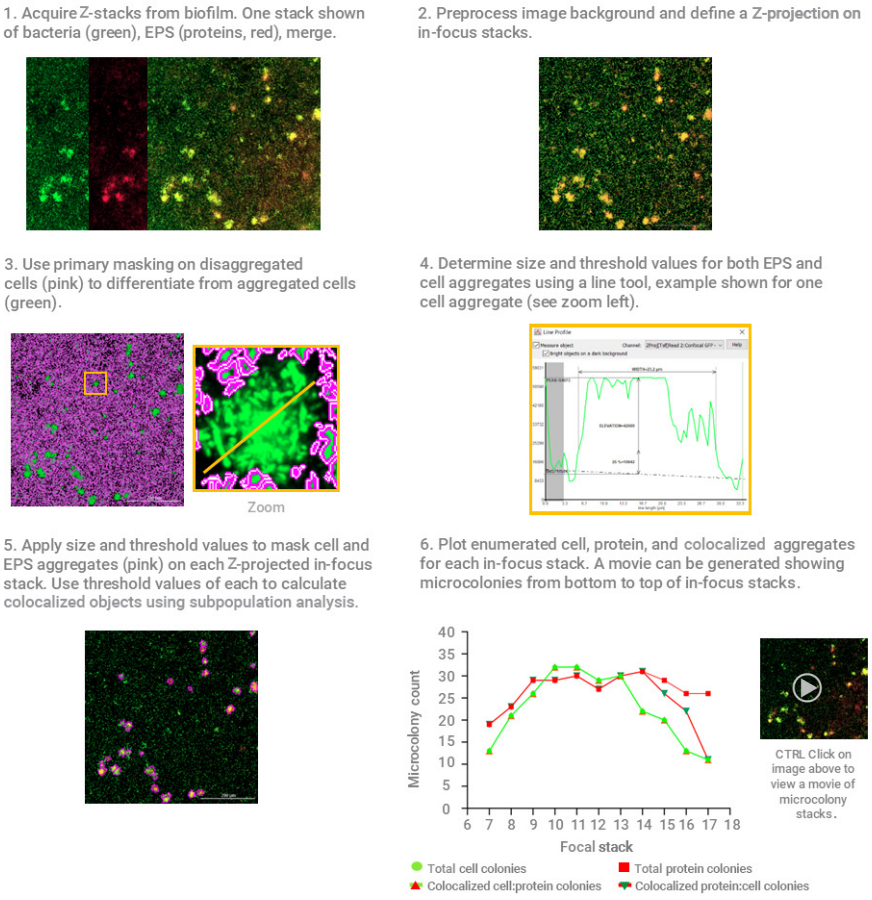

Figure 10. Steps for identifying and enumerating microcolonies using the Agilent BioTek Cytation C10 confocal imaging reader and Agilent BioTek Gen5 Image Prime software confocal Z-stacking image analysis.

Conclusion

The Agilent BioTek Cytation C10 confocal imaging reader has capabilities conducive to integrating data acquisition and analysis from different detection and imaging methods, as demonstrated using biofilm assays as a model. Multiple bacterial strains, different experimental variables, and a variety of stains and vessels were analyzed by means of numerous configurations of absorbance and fluorescence detection and both widefield and confocal imaging modes, using multiple objective magnifications. This resulted in a variety of analysis outcomes informing on fundamental experimental optimization variables common to biofilm in vitro workflows, including determining cell density and viability of starting cultures, biofilm formation and total biomass screening, assessing qualities of biofilm substrate adherence, characterizing EPS and growth architecture from live biofilm imaging, and comparing antimicrobial tolerance of planktonic and biofilm bacterial cells. The instrument eliminates constraints that may be imposed by a single-purpose instrument. It has a configurable design with the potential to replace up to five individual devices and is controlled using one centralized user interface and data management format, all at a price point that offers significant value.

References

1. Ghannoum, M.; Parsek, M.; Whiteley, M.; Mukherjee, P. Editors, Microbial Biofilms, 2nd Edition. ASM Press, October **2015**. ISBN:9781555817459. *Microbial Biofilms, 2nd Edition | Wiley*.
2. Clinical Laboratory Standards Institute EP17-A2 standard Evaluation of Detection Capability for Clinical Laboratory Measurement Procedures; Approved Guideline-Second Edition, June **2012**.
3. Montanaro, L.; Poggi, A.; Visai, L.; Ravaioli, S.; Campoccia, D.; Speziale, P.; Arciola, C.R. Extracellular DNA in biofilms. *Int J Artif Organs*. **2011** Sep; *34*(9):824-31. DOI: 10.5301/ijao.5000051
4. Azeredo, J.; Azevedo, N.; Briandet, R.; Cerca, N.; Coenye, T.; Costa, A.R. et al. Critical review on biofilm methods. *Critical Reviews in Microbiology* **2017**, Vol 43, pgs 313-351. DOI: 10.1080/1040841X.2016.1208146
5. Wilson, C.; Lukowicz, R.; Merchant, S.; Valquier-Flynn, H.; Caballero, J.; Sandoval, J.; Okuom, M.; Huber, C.; Brooks, T.D.; Wilson, E.; Clement, B.; Wentworth, C.D.; Holmes, A.E. Quantitative and Qualitative Assessment Methods for Biofilm Growth: A Mini-review. *Res Rev J Eng Technol.* **2017** Dec; *6*(4) PMID: 30214915
6. Guzman-Soto, I.; McTiernan, C.; Conzalez-Gomez, M.; Mah, T-F.; Griffith, M.; Alarcon, E. et al. Mimicking biofilm formation and development: Recent progress in in vitro and in vivo biofilm models. *iScience* 24, **2021** May 21, 102443, pgs 1-51. DOI: 10.1016/j.isci.2021.102443
7. Flemming, H-C.; Wuertz, S. Bacteria and archaea on Earth and their abundance in biofilms. *Nat Rev Microbiol* 17, 247-260 (**2019**). DOI: 10.1038/s41579-019-0158-9
8. Vert. M. et al. Terminology for biorelated polymers and applications (IUPAC recommendations 2012). *Pure Appl. Chem.* (**2012**) 84, 377-410. DOI: 10.1351/PAC-REC-10-12-04
9. New, T.R.; Manz, B.; Volke, F.; Dynes, J.J.; Hitchcock, A.P.; Lawrence, J.R. Advanced imaging techniques for assessment of structure, composition, and function in biofilm systems. FEMS Microbiol Ecol. **2010** Apr; *72*(1):1-21. DOI: 10.1111/j.1574-6941.2010.00837.x
10. Schlager, S.; Meyer, R.L. Confocal microscopy imaging of the biofilm matrix. *Journal of Microbiological Methods* 138, **2017**, pgs 50-59. DOI: 10.1016/j.mimet.2016.03.002
11. Penesyan, A.; Paulsen, I.T.; Kjelleberg, S.; and Gillings, M.R. Three faces of biofilms: a microbial lifestyle, a nascent multicellular organism, and an incubator for diversity. npj *Biofilms and Microbiomes* **2021**, Volume 7 Article Number 80, pgs 1-9. DOI: 10.1038/s41522-021-00251-2
12. Zhang, Y-Q; Ren, S-H; Li, H-L, et al. Genome-based analysis of virulence genes in a non-biofilm-forming Staphylococcus epidermidis strain (ATCC 12228). *Molecular Microbiology* **2003** DOI: 10.1046/j.1365-2958.2003.03671.x
13. Marmont, L.S.; Whitfield, G.B.; Rich, J.D.; Yip, P.; Giesbrecht, L.B.; Stremick, C.A.; Whitney, J.C.; Parsek, M.R.; Harrison, J.J.; Howell, P.L. PelA and PelB proteins form a modification and secretion complex essential for Pel polysaccharide-dependent biofilm formation in *Pseudomonas aeruginosa*. *J Biol Chem.* **2017** Nov 24;*292*(47):19411-19422. DOI: 10.1074/jbc.M117.812842
14. Thi, M.T.T; Wibowo, D., Rehm, BHA. *Pseudomonas aeruginosa* Biofilms. *Int J Mol Sci.* **2020** Nov 17;*21*(22):8671. DOI: 10.3390/ijms21228671
15. Reichhardt, C.; Parsek, MR. Confocal Laser Scanning Microscopy for Analysis of *Pseudomonas aeruginosa* Biofilm Architecture and Matrix Localization. *Front Microbiol.* **2019** Apr 2; 10:677. DOI: 10.3389/fmicb.2019.00677

16. Okshevsky, M.; Meyer, R.L. The role of extracellular DNA in the establishment, maintenance, and perpetuation of bacterial biofilms. *Critical Reviews in Microbiology*, **2015**, 41:3, 341-353. DOI: 10.3109/1040841X.2013.841639

17. Sauer, K.; Stoodley, P.; Goeres, D.M.; Hall-Stoodley, L.; Burmolle, M.; Stewart, P.S.; and Bjarnsholt, T. The Biofilm life cycle: expanding the conceptual model of biofilm formation. *Nature Reviews, Microbiology* **2022**, *20*, 608-620. DOI: 10.3109/1040841X.2013.841639

18. Flemming, HC.; Wingender, J. The biofilm matrix. *Nature Reviews Microbiology* **2010**, *8*, 623-633. DOI: 10.1038/nrmicro2415

19. Sharma, G.; Sharma, S.; Sharma, P.; Chandola, D.; Dang, S.; Gupta, S.;Gabrani, R. Escherichia coli biofilm: development and therapeutic strategies. *J Appl Microbiol.* **2016**. Aug;*121*(2),309-19. DOI: 10.1111/jam.13078

20. Live/Dead BacLight Bacterial Viability Kits, Product Information Manual. Revised: 15-July-**2004**. Document Connect (thermofisher.com)

21. PrestoBlue HS Cell Viability Reagent Product Information Manual Rev. B.0. Document Connect (thermofisher.com)

22. Song, B.; Leff, L.G. Influence of magnesium ions on biofilm formation by *Pseudomonas fluorescens*, *Microbiological Research*, **2006**, *151*, Issue 4, 355-361. DOI: 10.1016/j.micres.2006.01.004

23. Oyarzúa Alarcón, P.; Sossa, K.; Contreras, D.; Urrutia, H.; Nocker, A. Antimicrobial properties of magnesium chloride at low pH in the presence of anionic bases. *Magnes Res.* **2014** Apr-Jun;*27*(2):57-68. DOI: 10.1684/mrh.2014.0362

24. Webb, M. The Influence of Magnesium on Cell Division 3. The Effect of Magnesium on the Growth of Bacteria in Simple Chemically Defined Media. *Microbiology*, **1949**, *3*(3), 418-424. DOI: 10.1099/00221287-3-3-418

25. Costerton JW, Lewandowski Z, Caldwell DE, Korber DR, Lappin-Scott HM. Microbial biofilms. *Annu Rev Microbiol*. **1995**, 49:711-45. DOI: 10.1146/annurev.mi.49.100195.003431

26. Merritt, J.H.; Kadouri, D.E.; O'Toole, G.A. (2006), Growing and Analyzing Static Biofilms. *Current Protocols in Microbiology*, 00:1B.1.1-1B.1.17. DOI: 10.1002/9780471729259.mc01b01s00

27. Allkja, J.; Charante, van F.; Aizawa, J.; Reigada, I.; Guarch-Perez, C.; et al. Interlaboratory study for the evaluation of three microtiter plate-based biofilm quantification methods. *Nature Scientific Reports* **2021** 11:13779. DOI: 10.1038/s41598-021-93115-w

28. O'Toole, G.A. Microtiter dish biofilm formation assay. *J Vis Exp.* **2011** Jan 30; (47):2437. DOI: 10.3791/2437

29. Crouzet, M.; Le Senechal, C.; Brozel, V.S.; Costaglioli, P.; Barthe, C.; Bonneu, M.; Garbay, B.; Vilain, S. Exploring early steps in biofilm formation: set-up of an experimental system for molecular studies. *BMC Microbiol.* **2014** Sep 30; 14:253. DOI: 10.1186/s12866-014-0253-z

30. Okshevsky, M.; Meyer, R.L. Evaluation of fluorescent stains for visualizing extracellular DNA in biofilms. *Journal of Microbiological Methods* **2014** 105, 102-104. DOI: 10.1016/j.mimet.2014.07.010

31. Flemming, HC.; Van Hullebusch, ED.; Neu, TR.; Nielsen, PH.; Seviour, T.; Stoodley, P.; Wingender, J.; Wuertz, S. The biofilm matrix: multitasking in a shared space. *Nat Rev Microbiol.* **2023** Feb;*21*(2): 21: 70-86. DOI: https://doi.org/10.1038/s41579-022-00791-0

www.agilent.com/lifesciences/biotek

DE87094723

Published in the USA, December 11, 2023
5994-6764EN

Agilent
Trusted Answers